SHIP-BRIDGE-PIER PROTECTIVE SYSTEMS

by

Akira Iwai[1], Hitoshi Nagasawa[2], Kazuki Oda[3] and Kuniaki Shoji[4]

ABSTRACT

This paper describes the analytical and experimental studies on the behaviors of a ship subjected to a sheering flow induced around a rectangular solid-type marine structure, and also deals with ship-structure protective systems against ship impacts.

Large bridge piers, which are constructed in a narrow waterway with strong tidal currents, are treated herein as one of the typical solid-type marine structures.

INTRODUCTION

Owing to the recent increase of marine traffic and marine structures such as bridge piers in navigable waters, ship collision accidents with the structures have been increasing.

The collapse accidents of the Tasman Bridge of Australia in 1975, the Tjorn Bridge of Sweden in 1980 and the Sunshine-Skyway Bridge of America in 1980 were brought about by the very ship collision.

The national big projects for bridge construction aiming to link the Shikoku Island to the Main Land of Japan are put into practice at the present or under planning at different three routs by the Honshu-Shikoku Bridge Authority.

Most of their piers are being constructed or planning to be constructed in narrow straits with strong tidal currents where numerous marine accidents have occured every year.

1 Professor of Navigation, Tokyo University of Mercantile Marine, Tokyo, Japan

2 Director of Ship Structure Division, Ship Research Institute, Tokyo, Japan

3 Associate Professor of Hydraulic Engineering, Osaka City University, Osaka, Japan

4 Associate Professor of Marine Engineering, Tokyo University of Mercantile Marine, Tokyo, Japan

When a solid-type structure comparably large to a ship size is places in strong tidal currents, sheering flows induced around the structures may cause serious navigational problems to the ships from the viewpoint of the safety maneuvering.

In this paper, bridge piers with a large rectangular cross section are treated as one of the marine structures, and the behaviors of ships navigating under the effects of sheering flows around the pier are predicted by means of an analitical method. And on the basis of the analytical results on the ship behaviors, the required minimum clearances between the ship courses and the pier to avoid collision accidents are proposed.

Moreover, the impact forces in the bow collision are estimated on the basis of the test results of the load-deformation characteristics of ship bows. And the load-penetration characteristics of proposed buffering devices are described.

SHIP BEHAVIORS NEAR THE PIER

Model experiments were carried out in a flow channel of Osaka City University, which is 35 m long, 4.0 m wide and 75 cm deep, to obtain the data of hydrodynamic exciting forces exerted on the ship due to sheering flows around the pier under conditions of reverse currents and zero ship speed.

One kind of ship model and three kinds of pier models were used. The length of the ship model was 100 cm. Though the length of the lateral side was maintained at 27 cm in all models, the length ratios of the longitudinal side to the lateral side, L_P/B_P, were varied 1.67, 2.00 and 2.33. The pier model of $L_P/B_P = 1.67$ was mainly used in the experiments. The length ratio of the lateral side of the pier model to the ship model, B_P/L_S, were varied 0.27 and 0.54.

The flow direction and the longitudinal axis of the ship model were kept normal to the lateral side of the pier model.

Hydrodynamic swaying forces and yawing moments on the ship model were measured by using dynamometers. And the hydrodynamic coefficients of swaying forces and yawing moments were obtained from Eqs. (1) and (2).

$$C_Y = Y_C / \frac{1}{2} \rho L_S d V^2 \tag{1}$$

$$C_N = N_C / \frac{1}{2} \rho L_S^2 d V^2 \tag{2}$$

where Y_C and N care respectively swaying forces and yawing moments, C_Y and C_N are coefficients of swaying forces and yawing moments; L_S and d are the length and the draft of the ship model; and V is the flow velocity; ρ is density of water.

Fig. 1 shows one example of the experimental results of the distribution of coefficients of swaying forces and yawing moments obtained from Eqs. (1) and (2) in case of $B_P/L_S = 0.27$ and $L_P/B_P = 1.67$. It may be said from Fig. 1 that both coefficients of swaying forces and yawing moments decrease exponentially with an increase of the dimensionless coordinates of the ship center x_0/B_P (or x_0/L_P) and y_0/B_P.
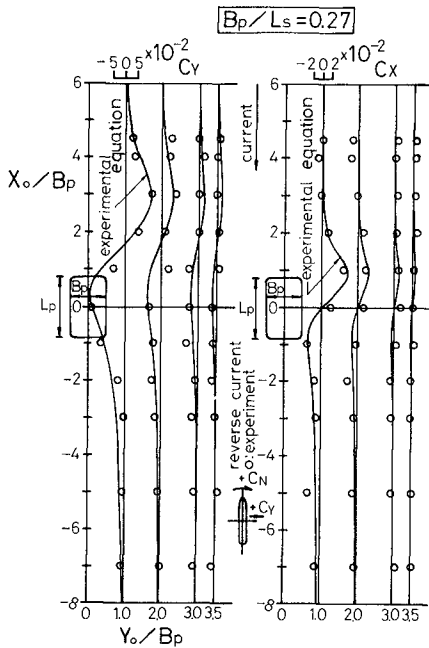
Fig. 1   Distribution of the hydrodynamic coefficients
of swaying forces and yawing moments

For the purpose of the estimation of coefficients of swaying forces
and yawing moments in numerical calculations of the ship motions, the
following empirical equations were derived as functions of x_0/L_p and
y_0/B_p on the basis of the whole experimental results.

$$
c_Y = \begin{cases} \dfrac{0.266 y_0/|y_0| \;\; (x_0/L_p - 1)\exp[-0.86(|y_0|/B_p - 1)]}{1 - (x_0/L_p - 1)^3} & \\ \qquad\qquad\qquad\qquad\qquad ; \; x_0/L_p \leq 1.0, \; y_0/B_p \geq 0.5 \\[2mm] \dfrac{0.196 y_0/|y_0| \cdot (x_0/L_p - 1)\exp[-0.86(|y_0|/B_p - 1)]}{1 + (x_0/L_p - 1)^4} & \\ \qquad\qquad\qquad\qquad\qquad ; \; x_0/L_p > 1.0, \; y_0/B_p \geq 0.5 \end{cases} \qquad (3)
$$

$$C_N = \begin{cases} \dfrac{0.110 y_0/|y_0| \cdot (x_0/L_p - 1)\exp[-0.98(|y_0|/B_p - 1)]}{1 + 4(x_0/L_p)^2} \\ \qquad\qquad\qquad\qquad\qquad ; \; x_0/L_p \leq 1.0, \; y_0/B_p \geq 0.5 \\[4pt] \dfrac{0.935 y_0/|y_0| \cdot (4x_0/3a)\exp[-0.98(|y_0|/B_p - 1)]}{1 + (4x_0/3L_p)^5} \\ \qquad\qquad\qquad\qquad\qquad ; \; x_0/L_p > 1.0, \; y_0/B_p \geq 0.5 \end{cases} \qquad (4)$$

where x_0 and y_0 are the coordinates of the ship center in $O\text{-}X_0Y_0$ coordinate system shown in Fig. 1.

The solid lines in Fig. 1 denote the coefficients estimated from Eqs. (3) and (4).

Substituting these hydrodynamic forces and moments estimated from the empirical equations as nonlinear external disturbances into the equations of ship maneuvering motions expressed by bymplified Eq. (5) and solving the equations of ship motions by numerical techniques, ship trajectories in the vicinity of the pier are obtained.

$$\left. \begin{aligned} (m + m_x)\dot{u} &= mvr \\ (m + m_y)\dot{v} &= Y_v v + (-mu + Y_r)r + y_\delta \delta + Y_C \\ (I_{zz} + J_{zz})\dot{r} &= N_v v + N_r r + N_\delta \delta + N_C \end{aligned} \right\} \qquad (5)$$

where m = mass of the ship; m_x and m_y = respectively added masses in sway and yaw motion; I_{zz} and J_{zz} = moment of inertia and added moment of inertia of the ship about the vertical axis through the center of ship gravity; u, $\dot{u}$, v, $\dot{v}$ = respectively components of the ship velocity and acceleration in X and Y axis direction(referred to Fig. 2); r and r = angular velocity and acceleration about the vertical axis; Y_v, N_v, Y_r and N_r = hydrodynamic coefficients concerning damping forces and moments respectively; Y_δ and N_δ = hydrodynamic coefficients of swaying forces and yawing moments induced by steering; δ = rudder angle; Y_C and N_C = exciting swaying forces and yawing moments given by Eqs. (1) and (2).

It was assumed in the caluculation that the ship comes up to the pier with an initial course pararell to the longitudinal side of the pier. Steering simulation was performed so as to give a rudder angle of 15 degrees to the occurence of yaw angle deviation of 2 degrees from the initial straight course.
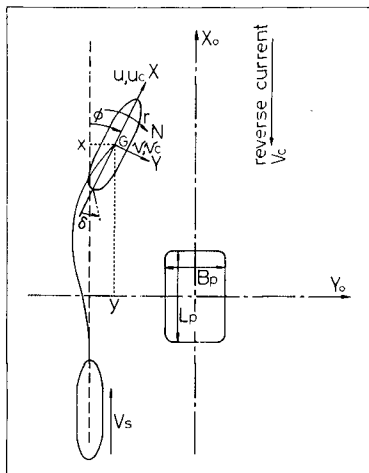
Fig. 2 Coordinate system

Values of added masses, added moment of inertias and other hydrodynamic coefficients concerning damping forces and moments used in the calculation are given in Table 1.

Table 1 Values of hydrodynamic coefficients used in the calculation of ship moments

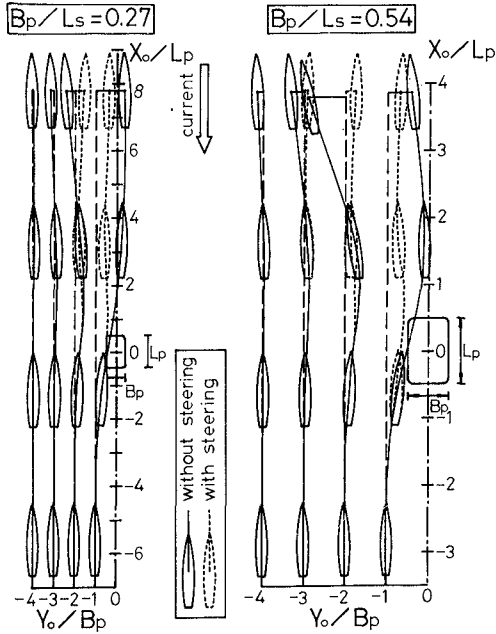| Swaying motion		Yawing motion	
$\dfrac{m + m_x}{\frac{1}{2}\rho L_s^{3}}$	0.018	$\dfrac{I_{zz} + J_{zz}}{\frac{1}{2}\rho L_s^{5}}$	0.0015
$\dfrac{Y_v}{\frac{1}{2}\rho L_s^{2}V}$	-0.01434	$\dfrac{N_v}{\frac{1}{2}\rho L_s^{3}V}$	-0.00460
$\dfrac{Y_r - mu}{\frac{1}{2}\rho L_s^{3}V}$	0.00456	$\dfrac{N_r}{\frac{1}{2}\rho L_s^{4}V}$	-0.00296
$\dfrac{Y_\delta}{\frac{1}{2}\rho L_s^{2}V^2}$	-0.00332	$\dfrac{N_\delta}{\frac{1}{2}\rho L_s^{3}V^2}$	0.00165

where V is the ship velocity relative to currents.

Fig. 3   Examples of the calculated ship trajectories (v_c/v_s = 0.75)

Fig. 3 shows two examples of the ship trajectories calculated under
the condition of v_c/v_s = 0.75 in the cases of B_p/L_s = 0.27 and 0.54
respectively.   Herein, v_c is the current velocity and v_s is the ship
velocity.

It can be said from Fig. 3 that the effect of sheering flow around the
pier on the ship course keeping becomes larger with an increase in
the length ratio of the lateral side of the pier to the ship, B_p/L_s.

REQUIRED SHIP COURSE CLEARANCE TO THE PIER

The maximum normalized sway deviation $\Delta y_m/L_s$ and yaw deviation $\Delta \phi_m$ from
the initial straight course are shown in Fig. 4 (a) and (b) respec-
tively for the case of B_p/L_s = 0.27 and B_p/L_s = 0.54 with respect to
the normalized coordinate of the initial ship course, y_0/B_p.   Herein,
Δy_m and $\Delta \phi_m$ are the maximum sway and yaw deviation caused within a
distance of one ship length away from the upstream side of the pier.

(a) $B_p/L_s = 0.27$ (b) $B_p/L_s = 0.54$
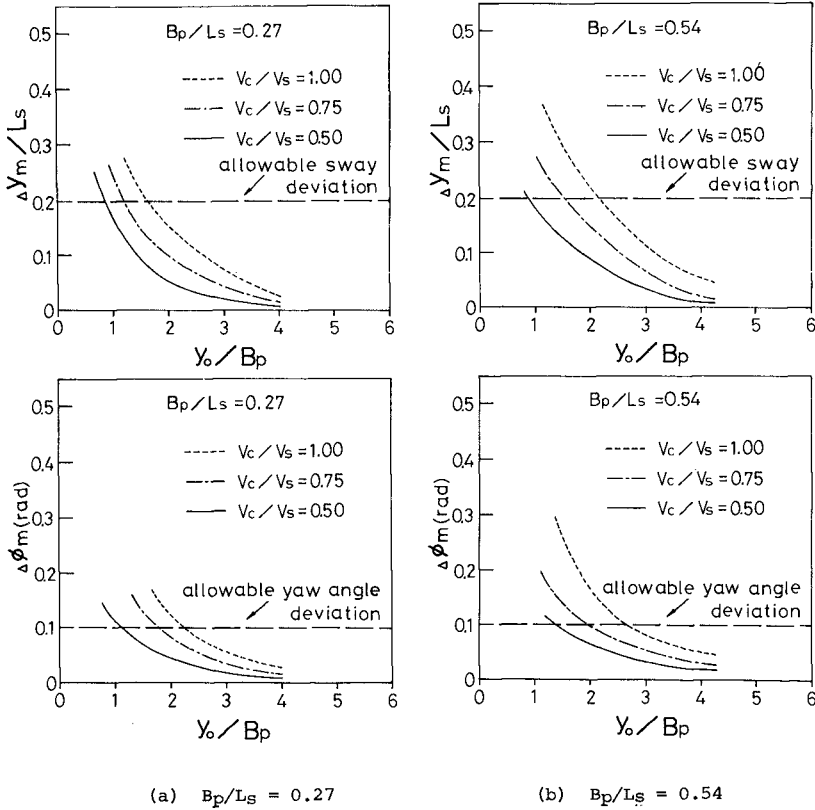
Fig. 4 Relationship between the maximum normalized sway deviation
and the normalized coordinate of the initial ship course

If the allowable deviation of ship motions from the initial course
are limited to 0.1 radian (about 5.7 degrees) in yaw angle and 0.2
time the ship length in sway displacement from the viewpoint of safety
ship handling, the minimum required distance of the ship course from
the pier center needed to avoid the collisions of the ship to ship
as well as the ship to pier may be determined in the manner which is
shown in Fig. 4 (a) and (b).

The minimum required distances from the pier center obtained in the
manner mentioned above are shown in a solid line for the case of
$B_p/L_s = 0.27$ and in a dotted line for the case of $B_p/L_s = 0.54$ in
Fig. 5.

It may be said from Fig. 5 that the minimum required distance become
larger with an increase in the velocity of tidal currents relative to
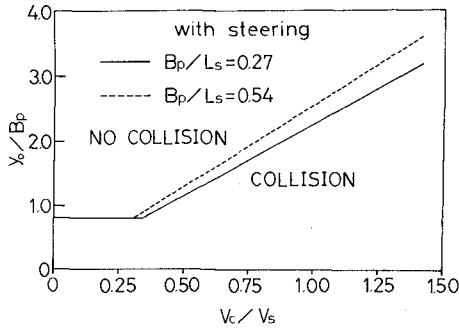the ship velocity.

Fig. 5 The minimum required distance of the ship course from the pier center

Fig. 5 is interpreted that for instance, when V_c/V_s = 1.0 in the case of B_p/L_s = 0.54, ships are recommended to navigate more than 2.6 times the length of lateral side of the pier away from the pier center in the distance. In other words, ships should pass near the pier having a clearance more than about 2.1 times the length of the lateral side from the longitudinal side.

COLLIDING FORMS OF THE SHIP

The behaviors of a drifting ship due to currents were experimentally obserbed in the vicinity of the pier by means of taking sequent pictures using a auto-driven camera.

(a) bow collision   (b) ship-side collision   (c) bow-shoulder collision
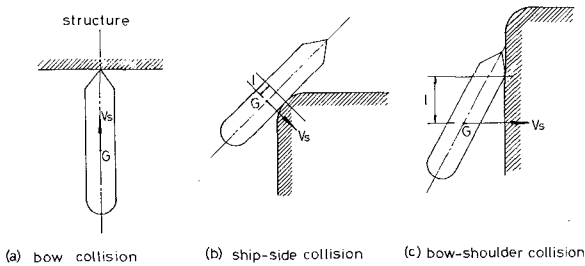
Fig. 6 Classification of the main colliding forms of the ship

Through the examinations of the ship behaviors in both navigating and
drifting near the pier obtained by means of the previous description,
colliding forms of the ship against the pier may be classified mainly
into three cases as shown in Fig. 6.

It may be said from the viewpoint of designing protective systems that
the most serious case is the bow collision among these colliding forms.

LOAD-DEFORMATION CHARACTERISTICS OF THE SHIP BOW

Static collapse tests were conducted to examine the load-deformation
characteristics using steel bow models which simulate the trans-
versely framed structure of cargo-type ships of 500 G.T. and 4,000 G.T.

The models are made in a scale of 1:4 for 500 G.T. ship and in a scale
of 1:8 for 4,000 G.T. ship.

For 500 G.T. ship, two kinds of bow models with a raked stem and with
a vertical stem while only one kind of model with the vertical stem was
used for 4,000 G.T. ship. The models with the vertical stem were used
for the simplification of the tests. Fig. 7 shows a diagram of the
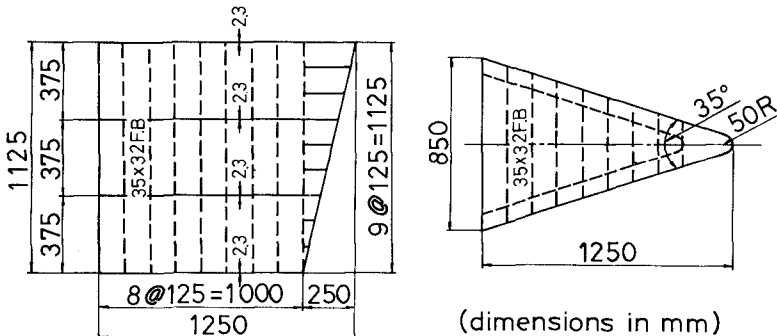one-fourth scale bow model of 500 G.T. ship with the raked stem.

Fig. 7 One-fourth scale bow model of 500 G.T. ship

Fig. 8 shows the test results of the load-deformation characteristics
of the 500 G.T. type bow model with the vertical stem in comparison
with the test results for the bow model with the raked stem. In
Fig. 8, a solid line denotes the test results for the case of the ver-
tical stem, and a broken line for the case of the raked stem.

It can be seen in Fig. 8 that there is little difference between the
load-deformation curves for the bow models with the raked stem and
with the vertical stem in the range of the deformation larger than the

length of the raked stem while the collapse loads near zero deformation show the great differences between them.
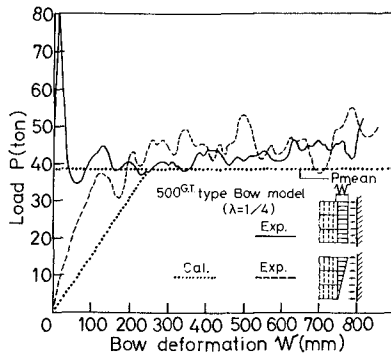

Fig. 8 Comparison between the load-deformation curves for two kinds of bow models of 500 G.T.

Fig. 9 also shows the characteristics of the load-deformation of one-eighth scale bow model of 4,000 G.T. with the vertical stem.
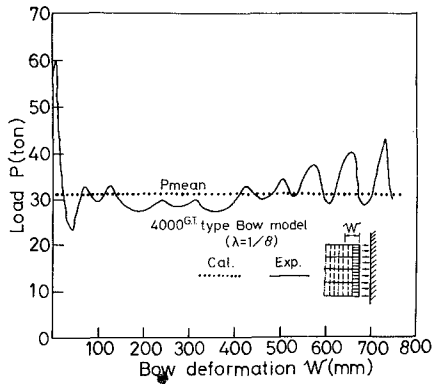

Fig. 9 Load-deformation curves of a one-eighth scale bow model of 4,000 G.T.

From these test results, it was found that the relationship between the
load and the bow deformation is characterized by the buckling strength
of a rectangular panel hull plate between the transverse flames (refer-
red to Fig. 10) and the load-bow deformation curve can be simplified
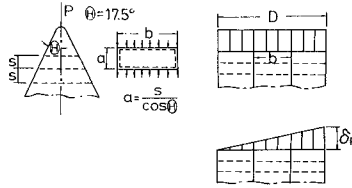and represented as shown in Fig. 11.

Fig. 10 Definition diagram of the
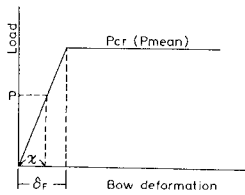rectangular panel hull plate

Fig. 11 Simplified load-bow deformation curve

In Fig. 11, δ_F is a raked stem length which is equal to about a quarter
of the depth in usual ships and P_{cr} is the component of a buckling load
of the rectangular panel hull plate of the bow in the direction of the
longitudinal ship axis which is expressed by Eq. (6)

$$P_{cr} = 2Dt \cos\theta \times \sigma_{cr} \tag{6}$$

where D = the depth of the ship; t = the thickness of the hull plate;
θ = the entrance angle of the bow; and σ_{cr} = the buckling stress of the
rectangular panel plate expressed by Eq. (7).

$$\sigma_{cr} = \kappa\left\{\pi^2 E/12(1 - \nu^2)\right\} (t/b)^2 \tag{7}$$

where $\kappa =$ buckling coefficient; E = Young's modulus; ν = Poisson's ratio; and b = the depth of the panel.

The dotted lines in Figs. 8 and 9 represent the calculated results by Eqs. (6) and (7) in comparison with the experimental results. Generally, it can be stated that the agreement between the calculated and the experimental results is satisfactory.

ESTIMATIONS OF THE IMPACT FORCES

Using the simplified load-deformation curve of the bow hull, ship impact forces can be estimated at the bow collision with a right angle against a vertical flat plane of a rigid bridge pier. The estimated results herein are graphically shown for the ship collision ranging from 500 G.T. to 4,000 G.T. in Fig. 12.
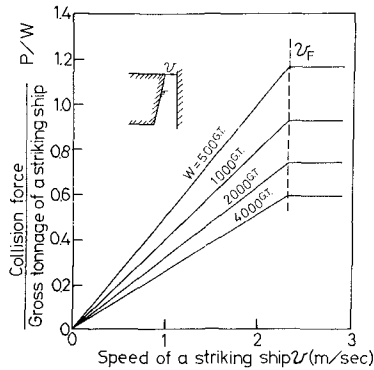

Fig. 12 Estimated impact forces at the bow collision

In Fig. 12, V_F is the speed of the striking ship resulting in the full collapse of the part of the raked stem. According to Fig. 12, V_F is equal to about 2.3 m/sec for every ship ranging from 500 G.T. to 4,000 G.T., and the maximum impact forces are estimated to be about 580 tons for the 500 G.T. ship and about 2,400 tons for the 4,000 G.T. ship.

Judging from the viewpoint of designing the ship-pier protection, it may be said that the striking ship speed should be less than the value of V_F using other detached-type fendering systems, or the impact forces should be reduced to the values less than the buckling loads of the bow hull plate by means of effective buffer devices installed on the pier. Herein, the ship-pier protective systems based on the latter idea were discribed.

PROPOSED BUFFER DEVICES AND THE FORCE-DEFORMATION CHARACTERISTICS

Four kinds of buffer devices were proposed which are coarse grid-type, dense grid-type, grid-composite-type filled up with hard polyerethane foam and composite-type filled up with hard polyurethane foam.

The schematic diagrams of the models of the proposed buffer devices are shown in Fig. 13 and the model dimensions of the coarse grid-type and the composite-type are shown in Fig. 14. The compressive strength of hard polyurethane foam used in the tests are 1.4 Kg/cm^2.
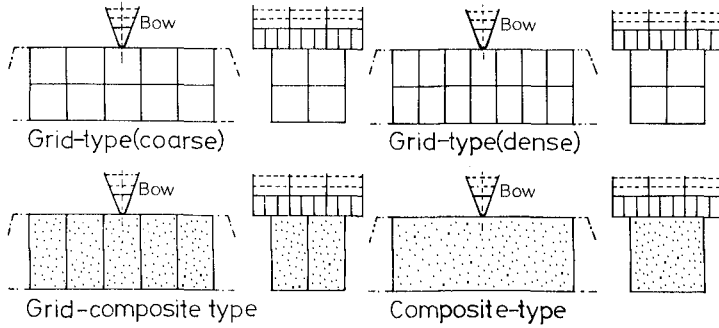

Fig. 13 Schematic diagram of the models of the proposed buffer devices
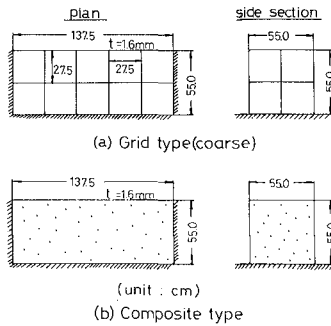

Fig. 14 Model dimensions of the coarse grid-type and the composite-type

The comparisons between the force-bow penetration curves for the pre-
ceding four kinds of buffer devices are shown in Fig. 15. They were
obtained from the static fracture tests performed by the use of a one-
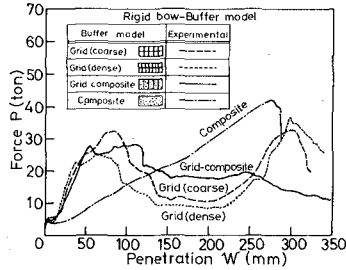eleventh scale rigid bow model of 4,000 G.T. ship.

Fig. 15 Comparisons between the force-bow penetration
curves for four kinds of buffer devices

It appears from Fig. 15 that the composite-type buffer device has almost
linear characteristics in the relationship between the force and the
ship penetration while other three kinds of buffer devices have some-
what complicate characteristics.

Every ship has a different bow collapse load because it depends on the
size and the structure of the bow itself. The composite-type buffer
device has the characteristic capable of absorbing the impact energies
in relatively small reactive forces. Therefore, it can be stated from
the viewpoint of practical designing that the composite-type is the
most suitable buffer device among the proposed ones.

It was found from the further static fracture tests using a elastic
bow model which simulates an actual bow that the linear superposition
of the independent load-deformation characteristics of the bow itself
and the buffer itself can be adapted for the estimation of the combined
load-deformation characteristics in the ship-buffer collision.

The composed deformations of the bow and the respective buffer devices
at the 4,000 G.T. ship collision were estimated in prototype values
on the basis of the test results as shown in Fig. 16.

Fig. 16 shows that the composite-type has much larger deformation in
comparison with the other three types. Fig. 17 shows the estimated
results of the impact forces versus the penetration at the 4,000G.T.
ship collision against the composite-type buffer device 4.0 m broad
in which t_0 and q represent the thickness of the steel plate of the

buffer and the compressive strength of hard polyurethan foam res-
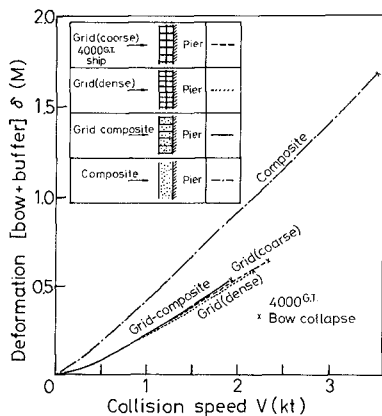pectively.

Fig. 16 Composed deformations of the bow and the respective
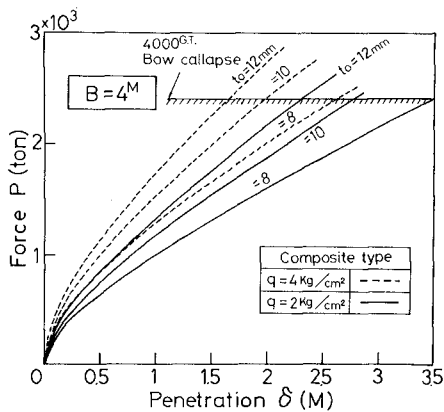buffer devices at the 4,000 G.T. ship collision

Fig. 17 Impact forces versus the penetration at the 4,000 G.T.
ship collision against the composite-type buffer device

SUMMARY AND CONCLUSIONS

In this paper, the behaviors of ships navigating under the effects of sheering flow around the solid-type bridge pier were predicted by means of the numerical analyses and the experiments in the flow channel.

Based on the previous predicted results, the minimum clearances between the ship course and the longitudinal side of the pier, which are required to avoid the ship-pier collision, were proposed.

The load-bow deformation characteristics for the ships ranging from 500 G.T. to 4,000 G.T. were examined by the bow collapse tests and were represented by the simplified equation.

Using the simplified load-bow deformation curve, the impact forces were estimated at the bow collision with a right angle against the vertical flat plane of the rigid bridge pier without any buffer devices.

The composite-type buffer device filled up with hard polyurethane foam was selected as the most suitable one among the proposed four kinds of buffer devices. And the impact forces at the 4,000 G.T. ship collision against the composite-type buffer device were estimated.

ACKNOWLEDGEMENT